Development of a Charge Estimator for Piezoelectric Actuators:
A Radial Basis Function Approach

Morteza Mohammadzaheri, Sultan Qaboos University, Muscat, Oman

Mohammadreza Emadi, Sultan Qaboos University, Muscat, Oman

 https://orcid.org/0000-0002-1127-1311

Mojtaba Ghodsi, Portsmouth University, Portsmouth, UK

Issam M. Bahadur, Sultan Qaboos University, Muscat, Oman

Musaab Zarog, Sultan Qaboos University, Muscat, Oman

Ashraf Saleem, Sultan Qaboos University, Muscat, Oman

ABSTRACT

Charge of a piezoelectric actuator is proportional to its displacement for a wide area of operating. Hence, a charge estimator can estimate displacement for such actuators. However, existing charge estimators take a sizable portion of the excitation voltage, i.e. voltage drop. Digital charge estimators have presented the smallest voltage drop. This article first investigates digital charge estimators and suggests a design guideline to (i) maximise accuracy and (ii) minimise the voltage drop. Digital charge estimators have a sensing resistor; an estimator with a constant resistance is shown to violate the design guideline; while, all existing digital charge estimators use one or a few intuitively chosen resistors. That is, existing estimators witness unnecessarily large inaccuracy and/or voltage drop. This research develops charge estimators with varying resistors, fulfilling the design guideline. Several methods are tested to estimates the sensing resistance based on operating conditions, and radial basis function network models excel in terms of accuracy.

KEYWORDS

Averaging, Charge, Digital, Interpolation, Nano-Positioning, Piezoelectric Actuator, Radial Basis Function Network, Voltage Drop

INTRODUCTION

Nano-positioning is an important area of nanotechnology, aiming at control of motion at nanometre scale. This area of technology has different applications such as scanning probe microscopy (Clayton, Tien, Leang, Zou, & Devasia, 2009) (including atomic force microscopy (Teh, 2015)), ultra-fine machining (Tang, Zeng, Gao, & Zhang, 2015) and medical engineering (including cell manipulation (Li

& Cheah, 2015) and robotic surgery (Saedi, Mirbagheri, Jafari, & Farahmand, 2014)). Various actuators have been used in nano/micropositioning e.g. worm gears (Protopopov, 2014) and magnetostrictive actuators (Ghodsi et al., 2016). Amongst all, piezoelectric actuators have the smallest size and the highest precision (Mohammadzaheri & AlQallaf, 2017). These actuators are the foremost actuators of nano-positioning at the moment and are likely to maintain this status for years (Moheimani, 2008).

Position control of (unfixed point(s)/surface(s) of) a piezoelectric actuator is the key task in piezo-actuated nano-positioning (Bazghaleh, Grainger, & Mohammadzaheri, 2018). Experiments have shown that charge of a piezoelectric actuator is proportional to its position/displacement for an extensive area of operating (Bazghaleh, Grainger, Cazzolato, & Lu, 2010; M. Bazghaleh, S. Grainger, M. Mohammadzaheri, B. Cazzolato, & T. Lu, 2013; Minase, Lu, Cazzolato, & Grainger, 2010; Yi & Veillette, 2005). This fact is the key motivation for design of charge estimators for piezoelectric actuators (Liu, Yen, & Wang, 2018; Mohammadzaheri & AlQallaf, 2017; Yang, Li, & Zhao, 2017).

All existing charge estimators need electrical element(s) (e.g. resistor(s) or capacitor(s)) in series with the piezoelectric actuator (Bazghaleh et al., 2018). The voltage across the aforementioned elements is not utilised to expand/contract the actuator; therefore, it should be minimised. This wasted voltage is called 'voltage drop' (Minase et al., 2010). Bazghaleh et al, showed that digital charge estimators cause less voltage drop than other existing charge estimators for piezoelectric actuators (M Bazghaleh et al., 2013).

However, as detailed in Problem Statement, design of existing digital charge estimators is partly intuitive. These inflexible and intuitively-designed estimators are shown to face a significant voltage drop or impreciseness if the area of operating is wide. This research addresses the aforesaid issue through development of intelligent charge estimators for piezoelectric actuators with varying resistors.

DIGITAL CHARGE ESTIMATORS

Figure 1 is a schematic of a digital charge estimator, used in this research. The estimator comprises of (i) a digital part, within the computer, (ii) an I/O card including analogue to digital (A/D) and digital to analogue (A/D) units, and (iii) analogue parts including the actuator, a voltage amplifier and a sensing resistor.

V_s, the voltage across the sensing resistor, is called the 'sensing voltage'. V_s is almost proportional to the current passing the actuator, i_P, and most of i_P passes through the grounded sensing resistor, R_s:

Figure 1. A schematic of the experimental setup used in this research
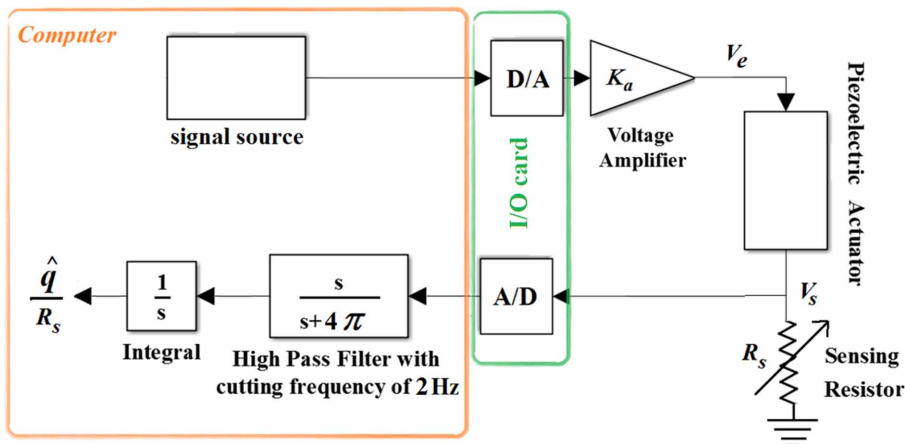
$$i_P \simeq \frac{V_S}{R_S} \tag{1}$$

Integral of i_p equals charge of the actuator; thus, theoretically, charge can be estimated with use of V_S.

However, integration of i_p is problematic. In practice, the analogue to digital converter, shown as A/D in Figure 1, is not ideal and has a minute offset voltage. This voltage together with dielectric leakage of the piezoelectric actuator generate a low frequency (almost constant) small bias voltage, V_b, which enters A/D along with V_S. This tiny bias voltage is accumulated through integration by the computer (left side of Equation (2)). Therefore, the calculated charge ($\hat{q}_P$) does not equal the real charge across the actuator (q_p):

$$\hat{q}_P = \int \frac{V_S + V_b}{R_s} dt \neq \int \frac{V_S}{R_s} dt \simeq q_P \tag{2}$$

This phenomenon is called drift (Bazghaleh, Mohammadzaheri, Grainger, Cazzolato, & Lu, 2013). The high pass filter, shown in Figure 1, supresses the low frequency bias voltage and prevents drift. Detrimentally, the high pass filter also suppresses low frequency components of V_S. As a result, a digital charge estimator does not suit low frequency operating areas.

PROBLEM STATEMENT

In this research, two rough design objectives of O1 and O2 are considered for digital charge estimators in the order of priority:

O1: High precision
O2: Low voltage drop

Resolution and input voltage range of A/D units of an I/O card play the major role in precision. Each A/D unit has n bits (resolution) and one or a number of range(s) for input voltage. For instance, an A/D may have 12 bits and its input range could be chosen from three options of ±0.625 V, ±2.5 V and ±10 V. Then, 2^n digital numbers is allocated to the input range of choice (Gray, 2006). The larger portion of the range covered by the input voltage (signal), the more digital numbers used to quantify the input signal, the higher precision. Hence, for a given resolution, maximum precision is achieved if input range of an A/D is fully used. V_S is the input to the A/D in digital charge estimators as depicted in Figure 1. Therefore, to achieve the highest precision, the range of V_S should be equal to an input range to the A/D of the I/O card; as a guideline to achieve O1.

Voltage drop, the portion of V_e not used for actuation, equals V_S. Thus, V_S can replace voltage drop in O2. Hence, V_S should be as small as possible, as a guideline to attain O1.

In summary, for a given I/O card, design objectives of O1 and O2 result in following design guidelines:

G1: The range of V_S should be equal to an input range of the I/O card.
G2: V_S should be as small as possible.

For a given I/O card, considering the higher priority of G1, both G1 and G2 can be combined as «Design Guideline: the range of V_S should be equal to the smallest input range of the I/O card».

This guideline guarantees the maximum precision at the smallest possible voltage drop. With a given excitation voltage (which depends on the required displacement) and I/O card, R_S, in Figure 1, is the only variable to tune V_S and meet the aforementioned guideline. However, experiments showed that a single value of R_S cannot satisfy the guideline across a wide area of operation. Figure 2 depicts V_S for the estimator of Figure 1 with a 5×5× 36 mm Piezo Stack of SA050536 type made by PiezoDrive Company (PiezoDrive, 2018) and R_S=100Ω for two excitation voltages 10sin(20×2πt)+10 V and 10sin(50×2πt)+10 V with a phase of -90°. The minimum input range of the I/O card is ±0.625 V. At the excitation frequency of 50 Hz, the selected value of R_S leads to use of a large portion of the input range and nearly fulfils the guideline. However, at 10 Hz, 55% of input range is left unused and the guideline is not met.

Figure 2 shows that a digital estimator with a single value of R_S does not suit a wide range of piezoelectric actuators' operation. However, all reported digital charge estimators of piezo-actuated nano-positioning systems have either a single value (M. Bazghaleh, S. Grainger, M. Mohammadzaheri, B. Cazzolato, & T.-F. Lu, 2013; Mohsen Bazghaleh, Morteza Mohammadzaheri, et al., 2013) or only a few instinctively chosen values of R_S (M Bazghaleh et al., 2013). This research proposes charge estimators with an adaptive R_S. An adaptive charge estimator, with a given I/O card, requires a mathematical model (F in Equation (3)) to determine the right R_S at any operating condition so as to fulfil the design guideline:

$$R_S = F \text{ (operating conditions)} \tag{3}$$

where operating conditions are waveform, amplitude (in V) and frequency (in Hz) of excitation voltage (V_e in Figure 1).

This research only deals with sinusoidal excitation voltages. Thus, the operating conditions are limited to amplitude (A_e) and frequency (f) of excitation voltage:

$$R_S = F(A_e, f) \tag{4}$$

Figure 2. The range of sensing voltage for same excitation amplitude of 10 V and different excitation frequencies of 10 and 50 Hz. The actuator is PZT with dimensions of 5×5× 36 mm.
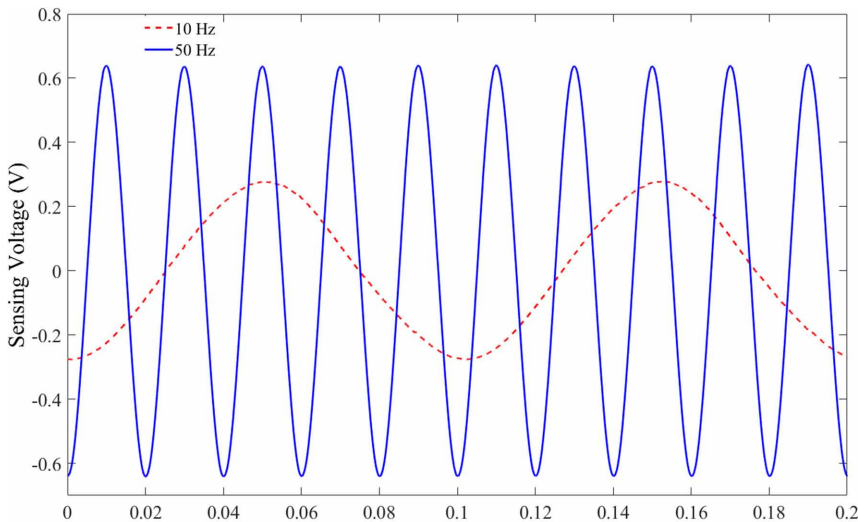
After identification of F, Equation (3) (or Equation (4)) will tune R_S to realise an adaptive charge estimator. Next two sections aim at identification of F using approximate analytical models and radial basis function networks, respectively.

EXPERIMENTATION

Figure 3 depicts the experimental setup, which is the implementation of Figure 1. The digital controller is a personal computer equipped with MATLAB 7.10 /Simulink 7.5 software including Simulink Real-Time Desktop Toolbox 3.5. The actuator is a 5×5×10 mm piezo stack, and the amplifier is MX-200, both made by made by PiezoDrive Company (PiezoDrive, 2018). A multifunctional card of Advantech PCI-1710U was employed to connect the computer and analogue parts. This card has a resolution of 12 bits and five optional ranges for analogue inputs ±10, ±5, ±2.5, ±1.25 and ±0.625 V.

In order to assess/develop mathematical models, which play the role of F in Equation (4), 35 series of experiments were performed. In all experiments, sinusoidal excitation voltages (V_e) with frequency of f (in Hz) and identical amplitude and bias of A_e (in V) were used:

$$V_e = A_e \sin(f \times 2\pi t) + A_e \tag{5}$$

where t is time in s. The values of 5, 10, 20, 30 or 40 V and 20, 30, 40, 50, 60, 70 or 80 Hz were used for A_e and f, respectively. In every experiment, the sensing resistance, R_S, was tuned so that the sensing voltage touches the range of ±0.625 V, minimum input range of the I/O card, then R_S was recorded. In other words, the value of R_S, with best matching to the design guideline, for each combination of excitation amplitude and frequency was experimentally found. The output of F in Equation (4) should ideally equal these results.

APPROXIMATE ANALYTICAL MODEL OF THE SENSING RESISTANCE

The purpose of this section is to analytically approximate F, presented in Equation (4). To do so, the piezoelectric actuator is approximated with a capacitor, C_p (M Bazghaleh et al., 2013), and tiny

Figure 3. Experimental setup
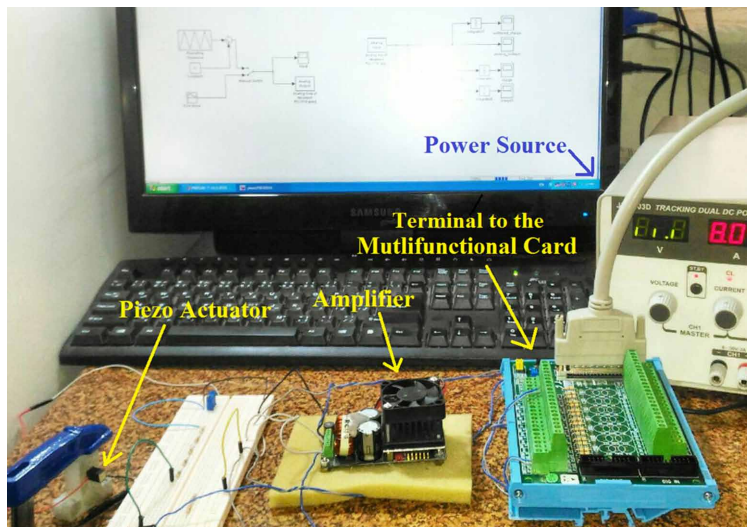
current entering the A/D card is neglected. Then, using Figure 3, combination of the actuator and the sensing resistor can be shown as Figure 4 (Mohammadzaheri et al., 2019).

For such an approximate system, in Laplace domain:

$$i_P(s) = \frac{V_e(s)}{R_S + \dfrac{1}{C_P s}} = \frac{V_S(s)}{R_S}$$

Consequently, the transfer function between the sensing voltage, V_S, and the excitation voltage, V_e, is:

$$\frac{V_S(s)}{V_e(s)} = \frac{R_S C_P s}{R_S C_P s + 1} \tag{6}$$

Model for Excitations Without Bias

For the approximate linear system presented by Equation (6), a sinusoidal excitation voltage without a bias, $V_e = A_e \sin\omega t$, leads to a sensing voltage of $V_S = A_S \sin\omega t$, where ω is frequency in rad/s, and the amplitude of A_S and A_e have the following relationship (Mohammadzaheri et al., 2019):

$$\frac{|V_S|}{|V_e|} = \frac{A_S}{A_e} = \left| \frac{R_S C_P j\omega}{R_S C_P j\omega + 1} \right| = \frac{R_S C_P \omega}{\sqrt{(R_S C_P \omega)^2 + 1}} \Rightarrow A_S \sqrt{(R_S C_P \omega)^2 + 1}$$
$$= A_e R_S C_P \omega \Rightarrow A_S^2 \left[(R_S C_P \omega)^2 + 1 \right] = A_e^2 (R_S C_P \omega)^2$$
$$\Rightarrow (R_S C_P \omega)^2 (A_e^2 - A_S^2) = A_S^2.$$

Consequently:

$$R_{SA} = \frac{A_S}{C_P \omega \sqrt{A_e^2 - A_S^2}} \tag{7}$$

where index A stands for analytically estimated. Considering the facts that (i) the smallest input range of the I/O card is ±0.625 V; that is, $A_S = 0.625$ V to meet the guideline detailed in Problem Statement, (ii) for the investigated actuator, $C_P = 1.046$ μF. Therefore:

Figure 4. Schematics of a resistor in series with a piezoelectric actuator which is assumed equivalent of a capacitor
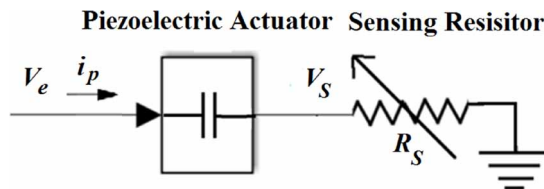
$$R_{SA} = \frac{0.5975 \times 10^6}{\omega\sqrt{A_e^{\,2} - 0.390625}} \tag{8}$$

where the unit for R_S is Ω. For $A_e >> 1$ and change of the unit of frequency from rad/s to Hz:

$$R_{SA} \simeq F_A(A_e, f) = \frac{0.95 \times 10^5}{A_e f} \tag{9}$$

Equation (9) is comparable with Equation (4).

Bias Effect

From Equation (8), $V_e = V_{ewb} + B$. With use of superposition, the sensing voltage can be assumed as sum of two components influenced by V_{ewb} and B (bias) excitations.

A component of V_S which is only influenced by B is presented as V_{SB}. Final value of V_{SB} is shown to be zero:

$$V_{SB}(s) = \lim_{s \to 0} s \frac{R_S C_P s}{R_S C_P s + 1} \frac{B}{s} = 0 \tag{10}$$

That is, the effect of bias disappears shortly; hence, bias has no enduring influence; thus, Equations (8) and (9) are still valid for excitations with a bias.

RBFN MODELS OF THE SENSING RESISTANCE

Radial basis function networks (RBFNs) were employed to approximate F in Equation (4). RBFNs are universal approximators with mathematically proven modelling capabilities (Mohammadzaheri, Chen, & Grainger, 2012; Mohammadzaheri, Ghodsi, & AlQallaf, 2018). In order to develop RBFNs, two separate series of data were employed: modelling and test data. Test data were not involved in identification of the model and merely used to cross-validate the RBFN models. Experiments provide 35 sets of data; each set includes two inputs (A_e and f) and a single output of R_S. The data with following couples of A_e (in V) and f (in Hz) were used for test: (10 70), (20 60), (30 50), (40 40) and (50 30). The rest of data, 30 sets, were used for modelling.

An RBFN has a two-layer mathematical structure, the first layer receives inputs array (U) and produces the 'layer output' (O). In this research, each column of U is $[A_e\ f\ ]^T$, where T stands for transpose. The second layer receives O and produces the 'network output' (Y). In this problem, Y is a row in which its elements are R_S.

The first layer has an array of weights, W, and a scalar namely spread, S. The components of layer output, O, are calculated as following:

$$O_{ik} = \exp\left(-\left(S\underbrace{\sum_{j=1}^{2}\left(W_{ij} - U_{jk}\right)^2}_{\substack{\text{distance between input} \\ \text{and weight arrays}}}\right)^2\right) \tag{11}$$

The second layer has two arrays of weights, X, and biases, B. The output array is calculated as following:

$$\hat{Y} = X \times O + B \tag{12}$$

Combination of Equations (11) and (12) is the RBFN; the next task is to identify unknown parameters of W, S, X and B using the modelling data, consisting of input and output arrays of $U_{2\times30}$ and $Y_{1\times30}$. There are two approaches to accomplish this task 'exact' and 'efficient' RBFN modelling.

Exact RBFN Modelling

Equation (11) indicates that greater components of O are more influential on the network's output. In addition, Equation (12) shows that (i) the range of O components is [0 1] and (ii) if the ith row of W is identical to the kth column of U, then O_{ik} will be maximum, 1. In exact RBFN modelling, it was considered that $W=U^T$; as a result, if the inputs of modelling data are given to such an RBFN, all elements of O are 1. With the aforementioned assumption, the only remaining unknown of the exact RBFN are X and B. With use a known O and the modelling data, Equation (12) in the form of Equation (13) could be solved to obtain B and X and fully identify the model:

$$Y_{1\times30} = \begin{bmatrix} X & B \end{bmatrix}_{1\times60} \begin{bmatrix} O \\ I \end{bmatrix}_{60\times30} \tag{13}$$

where I is a unique matrix with size of 30×30.

In the case inputs of the modelling data are fed to the exact RBFN, the model produces the exact outputs of the modelling data, regardless of the value of S in Equation (11). This is the reason behind the title of 'exact' for such an RBFN. However, a serious concern about exact RBFNs is inaccuracy of estimation outside the modelling data. A large spread (S) can smoothen and generalise the network (Beale, Hagan, & Demuth, 2017).

Here is a pseudo-algorithm of exact RBFN modelling (to find W, X, B and S using the input and out arrays of the modelling data, $U_{2\times30}$ and $Y_{1\times30}$):

1. Set $W_{30\times2} = U^T_{2\times30}$;
2. Set $O_{30\times30}$ = ones (30×30);
3. Form Equation (13) with $Y_{1\times30}$ and O from step 2 and solve it to find $X_{1\times30}$ and $B_{1\times30}$;
4. Choose a large S (198 in this research) to generalise the developed RBFN.

Maximum number of data sets which can be fed into the developed RBFN is 30, for smaller inputs some elements of B are not used.

Exact RBFNs advantageously has a straightforward non-iterative parameter identification algorithm. However, this method creates models with too many parameters, 121 in this research, where only 30 modelling data sets, in total 90 pieces of input/output data, are available. Excessive number of parameters and focus of the algorithm on exact fitting to the modelling data increase the risk of 'overfitting' or lack of generality (Cawley & Talbot, 2010; Mohammadzaheri, Mirsepahi, Asef-afshar, & Koohi, 2007). Concerns have been raised on sufficiency of spread (S) to adequately generalise the area of validity of the exact RBFNs outside the operating areas where the modelling data have been collected from (Cawley & Talbot, 2010).

Efficient RBFN Modelling

An alternative to exact RBFN modelling is efficient modelling which may produce RBFNs with fewer parameters than exact RBFNs. In spite of exact RBFNs which employ the transpose of input array of modelling data, U^T, as the weight array, W, in efficient RBFN modelling, some columns of U are selected and transposed to form W. Thus, W is often smaller than U (Mohammadzaheri et al., 2018).

In order to select U columns to be used as W rows, first, every single column of U is transposed and tried as a single-row W. Then, its corresponding X and B are calculated using Equation (18), and an RBFN is created. The column of U leading to the smallest modelling error (*ME*) is selected, transposed and used as the first row of W, where:

$$ME = \frac{1}{30} \sum_{i=1}^{30} \left(Y_i - \hat{Y}_i \right)^2 \tag{14}$$

Afterwards, remaining columns of U are tested to find the one in which addition of its transpose to W leads to the largest drop in the modelling error. Transposed of such a column is added to W. This continues till the number of W rows (*R*) reaches its pre-defined maximum (R_{max}=30 in this research) or the modelling error reaches its predefined target (E_t=1.7 Ω^2 in this research); targeting a too small modelling error (e.g. 0) rises the chance of overfitting.

Here is a pseudo-algorithm of efficient RBFN modelling:

1. W = null, U$_{rem}$ = U, U$_{opt}$ = null, E = 1000 (a large number), ^{T}W = null (temporary weight matrix);
2. Choose a large S (126 in this research) to generalise the developed RBFN;
3. Choose R_{max} (30 in this research) and target modelling error, E_t (1.7 in this research);
4. Set $R = 1$;
5. Set $k = 1$;
6. Add transpose of kth column of U$_{rem}$ to W to form ^{T}W;
7. Calculate O from Equation (11) with U$_{2\times30}$ from the modelling data and ^{T}W$_{R\times2}$ and S defined in steps 6 and 2;
8. Solve $Y_{1\times30} = \begin{bmatrix} X & B \end{bmatrix}_{1\times(R+30)} \begin{bmatrix} O \\ I \end{bmatrix}_{(R+30)\times30}$ to find X$_{1\times R}$ and B$_{1\times30}$ (Y and O are available from the modelling data and step 7);
9. Find the Modelling Error (*ME*)s from comparison of $\hat{Y}$ (calculated from Equations (11) and (12)) and Y, with use of Equation (14);
10. if *ME* < *E*, then *E* = *ME* and U$_{opt}$ = U$_k$;
11. $k = k + 1$;
12. if $k \leq$ 30-R then go to 6;
13. Remove U$_{opt}$ from U$_{rem}$ and add it to W;
14. $R = R+1$;
15. if $R \leq R_{max}$ and $E > E_t$ then go to 5.

RESULTS AND DISCUSSION

Assessment of Approximate Analytical Model

Figure 5 compares analytically approximated and experimental sensing resistances for the whole experiments. It is obvious that analytical models overestimate the resistance, particularly at low frequencies. These too high sensing resistances, if implemented, would lead to too high sensing

voltages, surpassing the selected input voltage range of the A/D, i.e. ± 0.625 V. As a result, the sensing voltage would be saturated and charge estimation cannot be performed in full. As an alternative, a below 1 factor should be multiplied by analytically estimated sensing resistances to avoid saturation of the sensing voltage.

Comparison of Analytical and RBFN Models and Other Data-Based Methods

Using the algorithms presented in RBFN modelling section and the modelling data presented Experimentation section, an exact and an efficient RBFN were developed. The exact RBFN has an $S = 198$ and for the efficient one $S = 126$, both values of S were obtained with trial and error. In order to develop the efficient RBFN, the target modelling error $= 1.7$ Ω^2, leading to a network with $R = 22$. The data of RBFN models have not been fitted into Figure 5, because for the modelling data (30 sets detailed), RBFNs inherently present extremely high accuracy which cannot be trusted for cross-validation. Only five sets of test data, detailed in RBFN modelling section, were used for cross-valuation of RBFNs. Estimated values by the developed RBFNs for the test data and their comparison with experimental and analytically approximated sensing resistances is presented in Table 1. Resistances estimated through data interpolation and averaging have been also presented in the table. Different interpolation algorithms were tried, and cubic outperformed others and was opted.

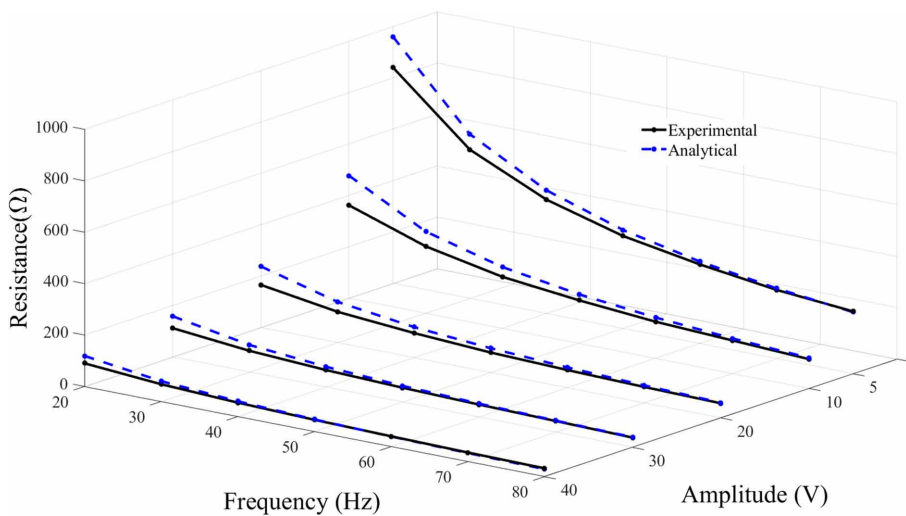**Figure 5. Experimental vs analytically approximated sensing resistance**

Table 1. Estimated sensing resistances by different models versus experimental values

Excitation Voltage (V)	Experimental R_S (Ω)	Estimated R_S (Ω)				
		Analytical Model	Exact RBFN	Efficient RBFN	Cubic Interpolation	Averaging
$5 \sin (2\pi \times 70t)$	267.9	273.9	266.2	265.8	275.7	198.4
$10 \sin (2\pi \times 60t)$	142.5	158.8	150.8	147.7	207.5	182.5
$20 \sin (2\pi \times 50t)$	78.5	95.1	76.7	77.4	81.2	106.2
$30 \sin (2\pi \times 40t)$	66.4	79.3	67.9	65.2	67.6	75.8
$40 \sin (2\pi \times 30t)$	67.2	79.3	59.3	67.7	70.2	84.8

Data interpolation results in fairly high accuracy at low frequencies, and a very bad estimation at the amplitude of 10 V and frequency of 60 Hz. Such an inaccurate estimation convinced authors to exclude interpolation from reliable estimation methods in this area of research. Averaging of available resistances of the immediate neighbouring operating areas did not result in accurate results as well. These show that data-based methods based on the data of adjacent operating areas cannot lead to accurate results, and techniques, such as RBFNs, which employ the whole data, are far more trustable.

Mean of absolute test error percentage, according to Equation (15), is 1.66%, 4.88%, 14.44%, 11.64% and 25.93% for efficient and exact and RBFNs, analytical model, interpolation and averaging, respectively. The mean of absolute test error is 2.01 Ω, 4.41 Ω, 12.77 Ω, 15.93 Ω and 32.84 Ω. Percentage-wise, interpolation presents better accuracy than the analytical model, due to better performance at lower sensing resistances. Furthermore, the efficient RBFN presents better estimation than the exact one in spite of having fewer parameters. For all test data sets, RBFNs outperform the analytical model. However, it should be noted that exact and efficient RBFNs have 121 and 97 parameters, respectively, while the analytical model has a single parameter:

$$\text{test error percent} = \frac{Experimental\ R_S - Estimated\ R_S}{Experimental\ R_S} \times 100 \tag{15}$$

CONCLUSION

This article started with a critical review of digital charge estimators for piezoelectric actuators. Based on this review, a design guideline was suggested for such estimators: for given excitation voltage and I/O card, the range of the sensing voltage should be equal to the smallest input range of the I/O card. Then, it was experimentally shown that an estimator with a fixed sensing resistor cannot satisfy the aforementioned guideline. However, all reported digital charge estimators of piezoelectric actuators use one or a few intuitively selected values for sensing resistance. Consequently, these estimators witness avertible accuracy loss and/or voltage drop. This research focuses to address this issue with use of variable resistance, determined with radial basis fountain models, in charge estimators.

A variety of methods were employed to estimate the sensing resistance so as the estimator meets the guidelines: (i) approximate analytical modelling, based on that assumption that a piezoelectric actuator behaves like a capacitor, (ii) radial basis function network (RBFN) modelling, a method of artificial intelligence, and (iii and iv) interpolation and averaging of experimentally-found sensing resistances around the operating area. RBFN provided models with highly accurate estimation. The best RBFN has an absolute maximum test error of 3.65% and mean of absolute error of 1.66%. Approximate analytical model always overestimates the resistance; however, the analytical model needs no experimental data and has only 1 parameters, while RBFN models have 97 and 121 parameters.

ACKNOWLEDGMENT

REFERENCES

Bazghaleh, M., Grainger, S., Cazzolato, B., & Lu, T.-f. (2010). An innovative digital charge amplifier to reduce hysteresis in piezoelectric actuators. *Paper presented at the Australian Robotics and Automation Association (ACRA)*, Brisbane, Australia. Academic Press.

Bazghaleh, M., Grainger, S., & Mohammadzaheri, M. (2018). A review of charge methods for driving piezoelectric actuators. *Journal of Intelligent Material Systems and Structures*, *29*(10), 2096–2104. doi:10.1177/1045389X17733330

Bazghaleh, M., Grainger, S., Mohammadzaheri, M., Cazzolato, B., & Lu, T. (2013). A digital charge amplifier for hysteresis elimination in piezoelectric actuators. *Smart Materials and Structures*, *22*(7), 075016. doi:10.1088/0964-1726/22/7/075016

Bazghaleh, M., Grainger, S., Mohammadzaheri, M., Cazzolato, B., & Lu, T.-F. (2013). A novel digital charge-based displacement estimator for sensorless control of a grounded-load piezoelectric tube actuator. *Sensors and Actuators. A, Physical*, *198*, 91–98. doi:10.1016/j.sna.2013.04.021

Bazghaleh, M., Mohammadzaheri, M., Grainger, S., Cazzolato, B., & Lu, T. F. (2013). A new hybrid method for sensorless control of piezoelectric actuators. *Sensors and Actuators. A, Physical*, *194*, 25–30. doi:10.1016/j.sna.2013.01.043

Beale, M., Hagan, M., & Demuth, H. (2017). *Neural Network Toolbox User's Guide.* Mathworks. Retrieved from https://www.mathworks.com

Cawley, G. C., & Talbot, N. L. (2010). On over-fitting in model selection and subsequent selection bias in performance evaluation. *Journal of Machine Learning Research*, *11*(Jul), 2079–2107.

Clayton, G. M., Tien, S., Leang, K. K., Zou, Q., & Devasia, S. (2009). A review of feedforward control approaches in nano-positioning for high-speed SPM. *Journal of Dynamic Systems, Measurement, and Control*, *131*(6), 061101. doi:10.1115/1.4000158

Ghodsi, M., Saleem, A., Özer, A., Bahadur, I., Alam, K., Al-Yahmadi, A., . . . Sheykholeslami, M. R. (2016). Elimination of thermal instability in precise positioning of Galfenol actuators. *Paper presented at the Behavior and Mechanics of Multifunctional Materials and Composites*. Academic Press.

Gray, N. (2006). *ABCs of ADCs*.

Li, X., & Cheah, C. C. (2015). Robotic cell manipulation using optical tweezers with unknown trapping stiffness and limited FOV. *IEEE/ASME Transactions on Mechatronics*, *20*(4), 1624–1632. doi:10.1109/TMECH.2014.2364620

Liu, S.-T., Yen, J.-Y., & Wang, F.-C. (2018). Compensation for the Residual Error of the Voltage Drive of the Charge Control of a Piezoelectric Actuator. *Journal of Dynamic Systems, Measurement, and Control*, *140*(7), 1–9. doi:10.1115/1.4038636

Minase, J., Lu, T. F., Cazzolato, B., & Grainger, S. (2010). A review, supported by experimental results, of voltage, charge and capacitor insertion method for driving piezoelectric actuators. *Precision Engineering*, *34*(4), 692–700. doi:10.1016/j.precisioneng.2010.03.006

Mohammadzaheri, M., & AlQallaf, A. (2017). Nano-positioning systems with piezoelectric actuators, current state and future perspective. *Science of Advanced Materials*, *9*(7), 1071–1080. doi:10.1166/sam.2017.3088

Mohammadzaheri, M., Chen, L., & Grainger, S. (2012). A critical review of the most popular types of neuro control. *Asian Journal of Control*, *16*(1), 1–11. doi:10.1002/asjc.449

Mohammadzaheri, M., Emadi, M., Ghodsi, M., Jamshidi, E., Bahadur, I., Saleem, A., & Zarog, M. (2019). A variable-resistance digital charge estimator for piezoelectric actuators: An alternative to maximise accuracy and curb voltage drop. *Journal of Intelligent Material Systems and Structures*, *30*(11), 1699–1705. doi:10.1177/1045389X19844011

Mohammadzaheri, M., Emadi, M., Ziaiefar, H., Ghodsi, M., Bahadur, I., Zarog, M., & Saleem, A. (2019). Adaptive Charge Estimation of Piezoelectric Actuators, a Radial Basis Function Approach. *Paper presented at the 20th International Conference on Research and Education in Mechatronics Wels*, Austria. Academic Press. doi:10.1109/REM.2019.8744122

Mohammadzaheri, M., Ghodsi, M., & AlQallaf, A. (2018). Estimate of the head produced by electrical submersible pumps on gaseous petroleum fluids, a radial basis function network approach. *International Journal of Artificial Intelligence and Applications*, *9*(1), 53–62. doi:10.5121/ijaia.2018.9104

Mohammadzaheri, M., Grainger, S., & Bazghaleh, M. (2013). A system identification approach to the characterization and control of a piezoelectric tube actuator. *Smart Materials and Structures*, *22*(10), 105022. doi:10.1088/0964-1726/22/10/105022

Mohammadzaheri, M., Mirsepahi, A., Asef-afshar, O., & Koohi, H. (2007). Neuro-fuzzy modeling of superheating system of a steam power plant. *Applied Mathematical Sciences*, *1*, 2091–2099.

Moheimani, S. O. R. (2008). Invited Review Article: Accurate and fast nano-positioning with piezoelectric tube scanners: Emerging trends and future challenges. *The Review of Scientific Instruments*, *79*(7). doi:10.1063/1.2957649

PiezoDrive. (2018). PiezoDrive Products. Retrieved from https://www.piezodrive.com

Protopopov, V. (2014). *Beam Alignment and Positioning Techniques. In Practical Opto-Electronics* (pp. 309–334). Springer. doi:10.1007/978-3-319-04513-9_10

Saedi, S., Mirbagheri, A., Jafari, A., & Farahmand, F. (2014). A local hybrid actuator for robotic surgery instruments. *International Journal of Biomechatronics and Biomedical Robotics, 3*(2), 100-105.

Tang, H., Zeng, Z., Gao, J., & Zhang, X. (2015). A flexible parallel nanopositioner for large-stroke micro/nano machining. *Paper presented at the International Conference on Manipulation, Manufacturing and Measurement on the Nanoscale (3M-NANO)*. Academic Press.

Teh, Y. H. (2015). *Labview Based Pid Algorithm Development for Z Motion Control in Atomic Force Microscopy*. UTAR.

Yang, C., Li, C., & Zhao, J. (2017). A Nonlinear Charge Controller With Tunable Precision for Highly Linear Operation of Piezoelectric Stack Actuators. *IEEE Transactions on Industrial Electronics*, *64*(11), 8618–8625. doi:10.1109/TIE.2017.2698398

Yi, K. A., & Veillette, R. J. (2005). A charge controller for linear operation of a piezoelectric stack actuator. *IEEE Transactions on Control Systems Technology*, *13*(4), 517–526. doi:10.1109/TCST.2005.847332

Morteza Mohammadzaheri completed his PhD in Intelligent Control at the School of Mechanical Engineering, University of Adelaide, Australia, in 2011. Dr Mohammadzaheri is currently an Assistant Professor of Dynamic Systems and Control, at Mechanical and Industrial Engineering Department of Sultan Qaboos University, Oman. He has published more 100 peer-reviewed journal and conference articles.

Mohammadreza Emadi is a Ph.D. candidate of Mechanical Engineering in the area of System Dynamics, Vibrations and Control at the Shahrood University of Technology, Iran.

Mojtaba Ghodsi (PhD) received his B.Sc. degree in mechanical engineering from Isfahan University of Technology in 1999, the M.Sc. degree in applied mechanics from Tehran Polytechnic in 2001 and continued his research as Ph.D. (2007) and JSPS postdoctoral fellow (2009) in Precision Engineering Department of the University of Tokyo, Japan. He commenced his academic career in Tarbiat Modares University in 2009. Currently, he is pursuing his career at Sultan Qaboos University, Oman in the department of Mechanical and Industrial Engineering. His main research interests include smart materials for actuators, sensors and energy harvesting, NDT and development of Mechatronics systems and devices. Dr. Ghodsi is a Member of the IEEE and International Society of Optics and Photonics (SPIE).

Issam M. Bahadur received the B.A.Sc. in mechanical engineering from Sultan Qaboos University, Muscat, Oman, in 2003, the M.A.Sc. degree in mechanical engineering from the University of Toronto, Toronto, Canada, in 2006. From 2006 to 2009, he was appointed as a Lecturer at Sultan Qaboos University, where he was involved with teaching, academic advising, and research. He completed the Ph.D. degree in mechanical engineering at the University of Toronto in 2013. He is currently Assistant Professor in the Dept of Mechanical and Industrial Eng., Sultan Qaboos University, Sultanate of Oman. His current research interests include micro-electro-mechanical systems (MEMS), instrumentations, industrial automation, and smart materials and vibration.

Musaab Zarog received a PhD from the University of Newcastle Upon Tyne (UK) in 2006, BEng in Mechatronics and MSc in Automation and Control. He is currently an Assistant Professor at Sultan Qaboos University. His research interests are MEMS/NEMS and mechatronics.

Ashraf Saleem is currently serving as an Assistant Professor at the Electrical and Computer Engineering Department in Sultan Qaboos University/Oman. He obtained his BSc in Computer Engineering from the Philadelphia University and MSc and PhD in Mechatronics Engineering from the DeMontfort University/England in 2006. His main research areas include: identification and control of dynamic systems, modelling and simulation, model-based robust control, and smart actuators.